HHS Public Access

Author manuscript

Neuron. Author manuscript; available in PMC 2020 February 20.

Published in final edited form as:

Neuron. 2019 February 20; 101(4): 738–747.e3. doi:10.1016/j.neuron.2018.12.022.

Ionotropic Receptors Specify the Morphogenesis of Phasic Sensors Controlling Rapid Thermal Preference in *Drosophila*.

Gonzalo Budelli[1,#], **Lina Ni**[1,2,#], **Cristina Berciu**[3,†,#], **Lena van Giesen**[1], **Zachary A. Knecht**[1], **Elaine C. Chang**[1], **Benjamin Kaminski**[4], **Ana F. Silbering**[5], **Aravi Samuel**[6], **Mason Klein**[4,6], **Richard Benton**[5], **Daniela Nicastro**[3,7,*], **Paul A. Garrity**[1,*,¶]

[1]National Center for Behavioral Genomics and Volen Center for Complex Systems Department of Biology, Brandeis University, Waltham, MA 02453 [2]School of Neuroscience, Virginia Tech, Blacksburg, VA 24061 [3]Rosenstiel Basic Medical Sciences Research Center, Department of Biology, Brandeis University, Waltham, MA 02453 [4]Department of Physics, University of Miami, Coral Gables, FL 33146, USA [5]Center for Integrative Genomics, Faculty of Biology and Medicine, University of Lausanne, Lausanne CH-1015, Switzerland [6]Department of Physics and Center for Brain Science, Harvard University, Cambridge, MA 02138 [7]Departments of Cell Biology and Biophysics, University of Texas Southwestern, Dallas, TX 75390-9039.

Abstract

Thermosensation is critical for avoiding thermal extremes and regulating body temperature. While thermosensors activated by noxious temperatures respond to hot or cold, many innocuous thermosensors exhibit robust baseline activity and lack discrete temperature thresholds, suggesting they are not simply warm and cool detectors. Here we investigate how the aristal Cold Cells encode innocuous temperatures in *Drosophila*. We find they are not cold sensors, but cooling-activated/warming-inhibited phasic thermosensors that operate similarly at warm and cool temperatures; we propose renaming them “Cooling Cells”. Unexpectedly, Cooling Cell thermosensing does not require the previously reported Brivido Transient Receptor Potential

[*]co-corresponding authors: Daniela Nicastro, Daniela.Nicastro@utsouthwestern.edu Paul Garrity, pgarrity@brandeis.edu.

[#]Equal contribution

[†]Current address: Microscopy Core Facility, McLean Hospital, Belmont, MA United States 02478

[¶]Lead contact: Paul A. Garrity National Center for Behavioral Genomics, Volen Center for Complex Systems Biology Department, Brandeis University MS-008, 415 South Street, Waltham, MA 02453., pgarrity@brandeis.edu; Telephone: 781-736-3127; FAX: 781-736-8161

Author contributions: G.B., L.N., C.B., L.v.G., Z.A.K., M.K., D.N. and P.A.G. designed experiments. G.B. performed genetics, electrophysiology and data analysis. L.N. performed genetics, immunohistochemistry, calcium imaging and data analysis. C.B. performed electron microscopy, L.v.G. and E.C. performed immunohistochemistry, A.S. and R.B. developed antisera, Z.A.K. performed calcium imaging and data analysis, B.K. performed data analysis. M.K. performed calcium imaging and data analysis. D.N. performed EM data analysis. P.A.G. performed data analysis. G.B., L.N., R.B., D.N. and P.A.G. wrote the paper with input from all authors.

Declaration of interests: The authors have no competing interests.

DATA AND SOFTWARE AVAILABILITY

Custom codes used in calcium imaging analysis are available for download: arista imaging code is available at https://github.com/masonklein/neurophys/

(TRP) channels. Instead, three Ionotropic Receptors (IRs), IR21a, IR25a and IR93a, specify both the unique structure of Cooling Cell cilia endings and their thermosensitivity. Behaviorally, Cooling Cells promote both warm and cool avoidance. These findings reveal a morphogenetic role for IR receptors, and demonstrate the central role of phasic thermosensing in innocuous thermosensation.

Graphical Abstract

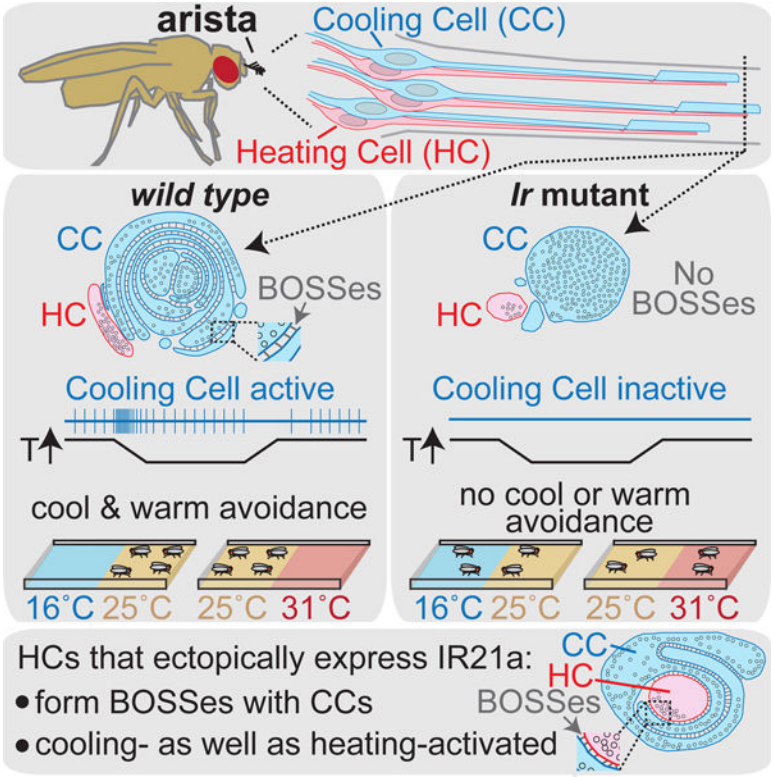

eTOC:

Budelli et al. find *Drosophila* thermoregulatory behavior is driven by a combination of heating and cooling detectors rather than hot and cold labeled lines. They further show Ionotropic Receptors not only confer thermosensitivity, they specify the thermoreceptor's complex dendritic morphology.

Keywords

thermosensation; thermoreceptor; temperature; sensory neuron; morphogenesis; Ionotropic Receptor; iGluR; Ir21a; Ir25a; Ir93a

Introduction

Animals rely on thermosensation to maintain appropriate body temperatures, avoid thermal extremes and, in vipers, bats, and blood-feeding insects, locate warm-blooded prey

(Bagriantsev and Gracheva, 2014; Vriens et al., 2014). From insects to vertebrates, thermosensing depends on multiple classes of thermosensors with distinct thermal sensitivities and behavioral roles (Barbagallo and Garrity, 2015; Palkar et al., 2015; Vriens et al., 2014). Thermosensors activated by noxious heat or cold commonly exhibit temperature thresholds beyond which they drive aversive responses. On the other hand, thermosensors responsive to innocuous temperatures commonly lack temperature thresholds. They instead exhibit robust baseline spiking and are more responsive to changes in temperature than its absolute value (Hensel, 1976; Palkar et al., 2015; Vriens et al., 2014). For example, in mammalian skin, innocuous cooling sensors primarily exhibit transient increases in firing upon cooling and decreases upon warming, and warming sensors the converse (Hensel, 1976). While it is clear that innocuous thermosensors have key roles in thermoregulation, how they encode temperature information and control thermoregulatory responses remains a major area of inquiry (Barbagallo and Garrity, 2015; Haesemeyer et al., 2018; Kamm and Siemens, 2017; Morrison, 2016).

The relative anatomical simplicity of the *Drosophila* thermosensory system has made it a powerful model for studying thermosensation (Barbagallo and Garrity, 2015). At the molecular level, multiple receptors have been implicated in innocuous thermosensing and behavioral thermoregulation in *Drosophila*. The Transient Receptor Potential (TRP) channel TRPA1 and the Gustatory Receptor (GR) GR28b mediate warmth-sensing in distinct sets of thermosensory neurons (Hamada et al., 2008; Ni et al., 2013), while adult cool-sensing has been reported to involve Brivido family TRP channels (Gallio et al., 2011). In addition, a trio of Ionotropic Receptors (IRs), IR21a, IR25a and IR93a, was recently shown to mediate the detection of cooling in the larva (Knecht et al., 2016; Ni et al., 2016). The IRs are a large family of invertebrate-specific sensory receptors related to variant ionotropic Glutamate Receptors (Croset et al., 2010). Many IRs have roles in chemosensing (Rytz et al., 2013), but a subset are involved in hygrosensing (Enjin et al., 2016; Frank et al., 2017; Knecht et al., 2017; Knecht et al., 2016) and thermosensing (Knecht et al., 2016; Ni et al., 2016). Among the IRs involved in thermosensing, IR25a and IR93a serve as co-receptors and act in multiple classes of sensory neurons, while IR21a appears specific for cooling detection (Knecht et al., 2016; Ni et al., 2016). How the information provided by these multiple classes of molecular receptors supports thermosensory behavior remains an open question.

At a cellular level, rapid responses to innocuous temperatures in *Drosophila* rely on peripheral thermosensors, including the Hot Cells and the Cold Cells (Gallio et al., 2011; Ni et al., 2013), named based on their putative hot- and cold-sensing abilities. Hot and Cold Cells are located in the arista, an extension of the antenna, and provide thermosensory input to target neurons in the antennal lobe of the fly brain (Frank et al., 2015; Liu et al., 2015). How *Drosophila* Hot and Cold Cells encode thermosensory information, including whether their activities primarily reflect absolute temperature (tonic signaling), temperature change (phasic signaling) or both (phasic-tonic signaling), has not been determined.

At an anatomical level, the sensory endings of Hot Cells and Cold Cells have very different morphologies (Foelix et al., 1989). Hot Cell outer segments are small and finger-like, while Cold Cell outer segments are large and terminate in elaborate lamellae, layers of infolded plasma membrane thought to contain the thermotransduction machinery (Foelix et al.,

1989). The extent of lamellation varies among Cold Cells within and between insect species, and correlates with a neuron's thermosensitivity (Altner and Loftus, 1985; Ehn and Tichy, 1996). Many vertebrate thermosensory neurons also have elaborate morphologies —from free nerve endings in mammalian skin to mitochondria-packed termini in rattlesnake pit organs (Goris, 2011; Munger and Ide, 1988; Wu et al., 2012). Despite the potential importance of these structures for thermotransduction, the molecules specifying them are unknown (Dong et al., 2015; Jan and Jan, 2010).

Here we use a combination of electrophysiology, molecular genetics, ultrastructure and behavior to determine how the *Drosophila* thermosensory system encodes thermosensory input and to identify key regulators of thermosensor development and function. These studies reveal that the Cold Cells are phasic detectors of temperature change, not cold sensors. Their steady-state activity does not increase at colder temperatures. Instead, they are transiently activated upon cooling and transiently inhibited upon warming, exhibiting this activity at temperatures both above and below the fly's preferred temperature. Furthermore, although activated by cooling, they mediate both warm and cool avoidance behavior. We suggest the Cold Cells be renamed "Cooling Cells" to accurately reflect their properties. At the molecular level, we find they rely upon a trio of IR family receptors (rather than the previously reported Brividos (Gallio et al., 2011)) to detect temperature, and ultrastructural analyses reveal a role for IR family sensory receptors in specifying sensory neuron morphogenesis as well as thermosensitivity.

Results

Cold Cells are cooling-activated phasic thermosensors

To assess thermosensory encoding in the arista, we established an electrophysiological preparation to monitor arista thermoreceptor spiking in response to discrete temperature steps. Prior studies have relied on calcium imaging, which reports relative rather than absolute levels of activity, limiting the ability to distinguish between tonic, phasic and phasic-tonic sensory encoding. Extracellular recording was performed through an opening created at the antennal arista tip, distal to thermoreceptor endings. The arista contains two classes of thermosensory neurons, originally called Cold Cells and Hot Cells. In wild-type animals, only the cooling-activated spikes of Cold Cells were readily observed (Fig. 1A, Supp. Fig. 1A). When detected, the warming-activated spikes of Hot Cells were ~4-fold smaller in amplitude; they were detectable above background only in rare preparations with highly favorable signal to noise (Supp. Fig. 2) or in animals whose Cold Cells were functionally compromised, as detailed below.

When exposed to alternating air streams of different temperatures (20˚C versus 25˚C or 25˚C versus 30˚C), Cold Cell activity transiently decreased during warming (often ceasing for a few seconds) and transiently increased during cooling (Fig. 1A). To further assess how Cold Cell spiking encodes thermosensory input, samples were held at constant temperature (30˚C) for ~120 sec to establish a stable baseline firing rate, cooled to 25˚C over ~4 sec, and subsequently held at 25˚C for another ~120 sec. Consistent with high thermosensitivity, Cold Cell spiking increased by >50% after an ~0.1˚ decrease (~0.52 seconds after cooling onset), reaching a peak spike rate of ~3 times baseline after an ~0.2˚C decrease (~0.65

seconds after cooling onset). Indicative of rapid adaptation, the response declined toward pre-stimulus levels even as the cooling ramp continued toward 25˚C (Fig. 1B, Supp. Fig. 1B). Importantly, Cold Cells did not exhibit tonic thermoreceptor activity. Steady-state spike rates of samples held at 30˚C and 25˚C were not statistically distinct; in fact, spike rates trended lower at 25˚C, the opposite of tonic cold receptor activity (102 +/− 20 (SEM, n=7) at 30˚C, 92 +/− 19 (n=7) at 25˚C). Thus, under the conditions examined, the Cold Cells behave as rapidly adapting, phasic thermoreceptors. Their activity is bidirectional, in that they are activated by cooling and inhibited by warming.

Cold Cells operated similarly at temperatures above and below the fly's preferred temperature of ~25˚C, as they also exhibited robust phasic responses to cooling from 25˚C to 20˚C (Fig. 1C, purple trace). The absence of tonic cold receptor activity was particularly apparent when comparing the spike rates of samples held at constant temperature for ~60 sec after a temperature change. For example, at this time point, preparations cooled to ~25˚C exhibited higher spike rates than preparations heated to ~25˚C (Fig. 1C, green and orange traces, respectively), demonstrating the persistent influence of prior exposure to cooling and warming. In addition, samples held at ~20˚C for ~60 sec after cooling had similar spike rates as samples held at ~30˚C for ~60 sec after heating, further demonstrating that Cold Cell spiking is not tightly coupled to absolute temperature (Fig. 1C, purple and pink traces, respectively). Together these data demonstrate that Cold Cells are not receptors for cool temperatures, at least under the conditions examined here. Rather they serve as phasic sensors whose activity reflects recent temperature change.

Cold Cell thermosensing is mediated by IR21a, IR25a and IR93a

Cold Cell thermosensing has been proposed to involve a set of TRP channels, the Brividos (Gallio et al., 2011). To gain further insight into their function, we assessed their impact on Cold Cell responses using electrophysiology. Surprisingly, we observed no alterations in Cold Cell thermosensitivity when testing the *brivido1* and *brivido2* mutants used in that prior study (Fig. 1D–F, Supp. Fig. 1C–F). To exclude assay details or strain contamination as explanations for the failure to observe a defect, calcium imaging was found to yield a consistent result (Supp. Fig. 1D–E) and the presence of the mutations was confirmed by DNA sequencing (Supp. Fig. 1F). One possible explanation for the discrepancy between these results and the prior report could be that genetic background differences among strains in the prior report altered GCaMP expression levels, yielding apparent reductions in response amplitude even though the neuron's underlying thermosensitivity was unchanged.

As Cold Cells showed no detectable requirement for Brividos to sense temperature, alternative receptors were sought. Cooling detection in *Drosophila* larvae depends on three Ionotropic Receptors (IRs), IR21a, IR25a and IR93a (Knecht et al., 2016; Ni et al., 2016). IR21a and IR25a expression has been detected in the arista (Benton et al., 2009) and adults lacking these IRs show altered thermal preferences (Enjin et al., 2016), making them promising candidates. To assess whether IR proteins might participate in Cold Cell thermotransduction, their distribution within the arista was examined. Immunostaining revealed robust concentrations of IR21a, IR25a and IR93a proteins in Cold Cell sensory endings, consistent with a role in thermosensing (Fig. 2). Expression of IR25a and IR93a,

but not IR21a, was also detected in Hot Cells (Fig. 2), consistent with the broader expression of the IR25a and IR93a co-receptors compared to cooling-specific IR21a. Immunostaining for each IR was eliminated in the corresponding mutant, confirming antisera specificity (Supp. Fig. 3).

Arista thermoreceptor responses were examined in *Ir21a*, *Ir25a* and *Ir93a* mutants. Consistent with an essential role for each of these IRs in Cold Cell thermosensing, the cooling-activated responses characteristic of Cold Cells were abolished in each *Ir* mutant (Fig. 3A, D, F, H, J **and** Supp. Fig. 4A, B). Rather than cooling-activated responses, each *Ir* mutant exhibited warming-activated spiking (Fig. 3A and Supp. Fig. 4A, B); this was subsequently found to come from the Hot Cell, whose activity is more readily detected in the *Ir* mutants. The phenotype of each *Ir* mutant was rescued using the corresponding wild-type transgene, confirming specificity (Fig. 3A, E, G, I, J). Cold Cell responses were unaffected in *Gr28b* mutant animals, whose Hot Cells are not thermosensitive, indicating that Hot and Cold Cell thermosensitivity are functionally independent (Fig. 3A, B, J). To confirm that the warmth-activated spiking observed in the *Ir* mutants reflected Hot Cell activity, *Ir21a,Gr28b* double mutants, in which the Hot Cell is not thermosensitive, were examined. Indeed, responses in the *Ir21a,Gr28b* double mutants animals completely lacked thermosensitivity (Fig. 3A, C, J). The results of these electrophysiological analyses were confirmed using calcium imaging. Thermosensitive Cold Cell responses, monitored using the genetically encoded calcium indicator GCaMP6m, were dramatically reduced in *Ir21a*, *Ir25a* and *Ir93a* mutants, while Hot Cell responses were unaffected (Supp. Fig. 4C, D). Thus, IR21a, IR25a and IR93a are specifically required for Cold Cell thermosensing.

As noted above, Hot Cell spikes were rarely detected in wild type recordings, but readily visible in *Ir* mutants. Calcium imaging revealed no decrement in Hot Cell responses in any of the *Ir* mutants (Supp. Fig. 4C, D), so we analyzed Hot Cell spiking in greater detail in one *Ir* mutant, $Ir93a^{-/-}$. Hot Cells exhibited robust phasic thermosensitivity, with warming eliciting transient increases in spiking and cooling transient decreases in spiking (Supp. Fig. 4B, Supp. Fig. 5A, B). The response was highly thermosensitive (though less thermosensitive than the Cold Cell response), as warming of ~2.5 to 3˚C resulted in an ~3-fold increase in Hot Cell spiking (Supp. Fig. 5C). In contrast to the Cold Cells, which were purely phasic, the Hot Cells also exhibited tonic thermosensory responses (Supp. Fig. 5B). When held at constant temperature, steady-state Hot Cell spiking was temperature dependent: 17 +/− 3 Hz at 20˚C (n=7, mean +/− SEM), 37 +/− 6 at 25˚C (n=14), and 74 +/− 17 at 30˚C (n=7) (30˚C distinct from 20˚C, alpha = 0.01, Tukey HSD). This corresponds to a Q10 of ~4.4, which is modest, but larger than the mean Q10 of ~2.3 for biological processes (Dell et al., 2011). Together, these data show that Hot Cell activity reflected a combination of recent temperature change and absolute temperature, at least under the conditions assayed here.

IRs are required for Cold Cell sensory ending organization

As the Cold Cells possess large and morphologically elaborate sensory endings (Altner and Loftus, 1985; Foelix et al., 1989), we examined whether Cold Cell morphology was visibly altered by IR loss. This seemed a possibility as IR loss both abolished Cold Cell spiking and

permitted the observation of Hot Cell spiking (Fig. 3), as might be predicted if Cold Cell dendrite morphology were affected. Thermoreceptor sensory endings were initially examined by fluorescence immunostaining for beta-tubulin as microtubules are both enriched in Cold Cell sensory endings (Foelix et al., 1989) and readily identified in electron micrographs, permitting correlation between light and electron microscopy. In wild-type tissue, three thick regions of tubulin staining were detected, corresponding to three arista sensilla each containing microtubule-rich thermoreceptor dendrites (Fig. 4A). IR21a staining overlapped and extended distal to each tubulin-rich region, consistent with IR21a's enrichment in the outer segment of the Cold Cell sensory ending. In *Ir21a* mutants, not only was IR21a immunostaining absent, tubulin staining was greatly reduced (Fig. 4A). *Ir25a* and *Ir93a* mutant phenotypes were similar to one another, but less severe than the *Ir21a* phenotype: in both *Ir25a* and *Ir93a* mutants, three discrete regions of tubulin staining were present, but the distal concentration of IR21a protein was absent (Fig. 4A).

To examine the morphological impact of IR loss at higher resolution, we used transmission electron microscopy of samples that were structurally well preserved by high-pressure-freezing/freeze-substitution. In wild type, each arista sensillum contains one Hot Cell and one Cold Cell, and each thermoreceptor extends a dendrite with a short ciliary region from which protrudes a morphologically distinct outer segment (Fig. 4B) (Foelix et al., 1989; Gallio et al., 2011). The Hot Cell outer segment has a simple finger-like shape, 200–300 nm in diameter, which flattens distally (Fig. 4B, red cell). In contrast, the Cold Cell outer segment is >500 nm across and highly convoluted, containing multiple closely packed membrane lamellae (Foelix et al., 1989) (Fig. 4B, blue cell), which have previously been correlated with thermoreceptive function (Altner and Loftus, 1985; Ehn and Tichy, 1996). These Cold Cell lamellar membranes are uniformly spaced apart (Fig. 4B), and the ~20 nm wide extracellular gap between lamellar membranes contains regularly spaced structures connecting the two membranes called "Bossy Orthogonal Surface Substructures" (BOSSes) (Steinbrecht, 1989) (Supp. Fig. 6).

Consistent with the results of light microscopy, ultrastructural analysis revealed that IR loss dramatically altered Cold Cell outer segment morphology. In *Ir25a* mutants, the Cold Cell ciliary region was present, but while the outer segment was large and microtubule-filled, it contained no lamellae or associated BOSS structures (Fig. 4C). *Ir21a* mutants exhibited even stronger defects: while a ciliary region was detected, only a rudimentary outer segment without microtubules or lamellae was observed (Fig. 4D). In contrast, Hot Cell dendrites exhibited no significant alterations in morphology in either mutant (Fig. 4C–D). These observations are consistent with the tubulin staining patterns observed by light microscopy (Fig. 4A), and demonstrate an essential role for IRs in the organization of the Cold Cell sensory ending.

IRs specify the structural organization of the Cold Cell sensory ending

Ectopic IR21a expression in the Hot Cells (which endogenously express IR25a and IR93a) is sufficient to render them responsive to cooling in addition to warming (Ni et al., 2016). The requirement for IRs in Cold Cell morphogenesis prompted us to examine whether IR21a misexpression also affected Hot Cell morphology. In wild type, Hot Cell and Cold Cell outer

segments often touch, but do not intermingle. Furthermore, at sites of contact, their membranes lie immediately adjacent, with neither the ~20nm separation nor BOSS structures of Cold Cell lamellae (Fig. 4B). Strikingly, when IR21a was expressed not just in the Cold Cell, but also in the Hot Cell, the Hot Cell outer segment became enwrapped by the Cold Cell outer segment as it extended distally (Fig. 5A). In addition, rather than lying immediately adjacent as in wild type (Fig. 5B, panel 1), sites of Hot and Cold Cell membrane contact exhibited both the uniform ~20 nm separation normally observed only in Cold Cell lamellae, and the regular arrays of BOSS-like structures in the extracellular space between them (Fig. 5B, panels 2 and 3). The morphological transformation of the sensory ending was highly selective, as IR21a-expressing Hot Cell outer segments remained smaller and finger-like (Fig. 5B). IR21a's ability to promote the enwrapping and structured association of outer segment membranes demonstrates this IR is a critical contributor to thermoreceptor morphogenesis.

IR-mediated cooling detection is required for warm as well as cool avoidance

Drosophila thermal preference has been proposed to rely on a system of hot and cold labeled lines, in which Cold Cells specifically mediate cool avoidance and Hot Cells specifically mediate warm avoidance (Gallio et al., 2011). However, the bidirectional thermosensitivity of both Cold Cells and Hot Cells over wide temperature ranges prompted a re-evaluation of their contributions to behavior. Cool avoidance was assessed by allowing flies to choose between zones of ~16˚C and ~25˚C (Fig. 6A). As anticipated, *Ir21a, Ir25a* and *Ir93a* mutants exhibited reduced cool avoidance, indicating that IR-mediated thermosensing is critical for this behavior (Fig. 6A). In contrast, Hot Cell thermosensing was not required, as *Gr28b* mutants robustly avoided the cooler region (Fig. 6A). Surgical removal of the arista (which contains only six neurons, three Hot and three Cold Cells) also reduced cool avoidance (Fig. 6A). These data are consistent with the canonical view that cool avoidance involves Cold but not Hot Cells.

We next tested the relative contributions of Hot and Cold Cells to warm avoidance using zones of ~25˚C and ~31˚C. Surprisingly, *Gr28b* mutants, whose Hot Cells do not detect warming, only partially reduced warm avoidance in this assay (Fig. 6B). In contrast, arista ablation abolished this behavior, suggesting Cold Cells also contribute (Fig. 6B). Consistent with this notion, *Ir21a*, *Ir25a* and *Ir93a* mutants each abolished warm avoidance (Fig. 6B). The effects of *Ir* mutants were as strong as arista removal (Fig. 6B) and significantly stronger than in *Gr28b* mutants ($P<0.05$ versus *Gr28b* mutants, Steel with control), demonstrating a major contribution of these receptors to warm avoidance. These findings are consistent with the contribution of these IR-dependent phasic thermosensors to both warm and cool avoidance, and inconsistent with the notion that such thermotactic behavior is driven by hot and cold labeled lines.

Discussion

Animals from flies to humans show preferences for specific temperatures. While thermal preference could result from the combined effects of hot and cold sensing pathways, our findings indicate this is not the case in *Drosophila*. Instead, thermal preference depends on a

set of phasic thermosensors that respond to temperature change rather than hot or cold, and that participate in both warm and cool avoidance. Although originally named “Cold Cells” (a convention followed in the results section), our data show that they are not cold sensors. We therefore propose their name be changed to “Cooling Cells” to more accurately reflect their activity. An advantage of phasic over tonic sensors is that their consistent baseline activity helps ensure sufficient dynamic range is available to respond to small changes in temperature with large changes in firing rate across a range of baseline temperatures. Phasic thermosensors in the ant, for example, respond to milli-degree fluctuations in temperature over a wide range of innocuous temperatures (Ruchty et al., 2010). Such phasic thermosensing enables an animal retain sensitivity to small temperature changes as its overall thermal environment shifts.

A potential limitation of the Cooling Cells’ phasic nature is that their responses are similar both above and below the preferred temperature. As the relative desirability of cooling versus warming is different in these two conditions, interpreting Cooling Cell activity as signifying an improving or deteriorating situation likely requires additional thermosensory input. Such context-dependent interpretation of Cooling Cell activity is also suggested by their importance in avoiding both overly cool and warm temperatures, even though their responses to temperature are similar throughout the innocuous range. Consistent with the involvement of multiple thermosensors, the loss of Hot Cell thermosensitivity in *Gr28b* mutants alters warm avoidance, although the defect effect is partial, suggesting additional contributors.

The context-dependent interpretation of phasic thermosensory input is a potentially general challenge. For example, innocuous thermosensors in mammalian skin, particularly cooling-sensitive neurons, are primarily phasic (Hensel, 1976), raising similar concerns about how their activity is interpreted to trigger responses that either raise or lower body temperature. Interestingly, current evidence indicates that such peripheral input is combined with additional thermosensory input in the hypothalamus to control thermoregulatory responses (Kamm and Siemens, 2017; Morrison, 2016; Vriens et al., 2014). A potentially analogous scenario has also been observed in the nematode *C. elegans*. In this system, the bidirectional AFD thermosensor (Ramot et al., 2008) mediates both warm and cool avoidance (Mori and Ohshima, 1995), acting through circuits that receive input from additional sensory neurons (Biron et al., 2008; Kuhara et al., 2008).

The discovery that Cooling Cell thermosensing depends on IRs rather than Brividos provides a unified view of cooling sensation in *Drosophila* and potentially other insects. Recent work has shown that larval Dorsal Organ Cool Cells (DOCCs) require IR21a, IR25a and IR93a to detect cooling (Knecht et al., 2016; Ni et al., 2016), and that IR21a (along with its co-receptors) is not only necessary, but also sufficient to confer cooling-sensitivity when ectopically expressed in the Hot Cells (Ni et al., 2016). Taken together, these data indicate that the combination of IR21a, IR25a and IR93a constitute a major pathway for cooling detection. In addition, like the Cooling Cells, DOCC thermosensing shows no requirement for Brivido TRP channels (Ni et al., 2016). The cellular origin of the behavioral defects reported in *brivido* mutants remains unclear (Gallio et al., 2011; Ni et al., 2016).

Our electrophysiological analysis of arista thermoreceptors also demonstrates that “Hot Cells” are not simple hot sensors. Instead they are active at cool as well as warm temperatures, transiently responding to temperature changes in a robust and bidirectional manner (warming-activated/cooling-inhibited). To more accurately reflect their properties, we propose their name be changed to “Heating Cells”. In addition, their steady-state firing rates rise with temperature (Q10 ~4.4). Warming accelerates most processes, but such thermosensitivity lies near the 90th percentile of biological processes (Dell et al., 2011). Thus, while their tonic responses are less thermosensitive than their phasic responses, both could contribute to Heating Cell function.

The overlapping contributions of Heating and Cooling Cells to thermosensory behavior is consistent with recent physiological analyses that demonstrate interactions between cooling- and warming-responsive peripheral inputs in the fly brain (Liu et al., 2015). The involvement of both Heating and Cooling Cells in warm avoidance is in agreement with the regulation of warming-activated projection neurons by both peripheral warming and cooling inputs, the latter mediated via inhibitory interneurons (Liu et al., 2015). Furthermore, warm avoidance’s greater reliance on *Ir21a*-dependent cooling detection than *Gr28b*-dependent warming detection is also consistent with the larger observed contribution of cooling-responsive inhibition to the control of warming-activated projection neurons (Liu et al., 2015). For cool avoidance, the dependence on *Ir21a*-mediated cooling detection, but not *Gr28b*-mediated warming detection, mirrors the control of cooling-activated projection neurons by cooling-activated, but not warming-activated inputs (Liu et al., 2015). Together, these findings provide a consistent picture in which cooling- and warming-activated peripheral inputs are not equal but opposite influences. Instead, the two inputs potentially communicate distinct information to the thermosensory system, with the phasic Cooling Cells playing an essential role in both warm and cool avoidance, while Heating Cells show a narrower domain of influence on thermotactic behavior.

At the molecular level, the contributions of IRs to sensory detection have been viewed solely through their potential to act as stimulus-responsive ion channels (Benton et al., 2009; van Giesen and Garrity, 2017). Here we show that IRs are also key regulators of neuronal morphogenesis, demonstrating that IRs are necessary and sufficient to drive the formation of the specialized membrane-membrane contacts characteristic of Cooling Cell sensory endings. As IR family members also mediate olfaction, gustation and hygrosensation, it will be of interest to determine whether IR-dependent morphogenesis supports these other sensory modalities as well.

From an evolutionary perspective, thermosensory neurons with similar morphologies are found throughout arthropods (Altner and Loftus, 1985). This morphological conservation parallels the widespread conservation of IR21a, IR25a and IR93a sequences (Croset et al., 2010), raising the possibility that their role in morphogenesis could be an ancient and conserved feature of the IR family. How the IRs contribute to the formation of lamellae and BOSS elements is not yet known, nor is the mechanistic contribution of these structures to thermotransduction. As IR proteins concentrate in the lamellar region of the Cooling Cells, they potentially reside in or near these structures. However, additional Cooling Cell-specific factors likely contribute to lamellae formation, as the structural transformation of the

Heating Cell dendrite upon IR misexpression is only partial. Specifically, while IR21a misexpression converts Heating Cells into cooling-activated thermoreceptors (without affecting their warmth-sensitivity (Ni et al., 2016)) and promotes membrane contacts with the Cooling Cells, the Heating Cell dendrite remains finger-like and does not form internal lamellae. In addition, initial attempts to drive cell-cell association and dendritic remodeling by IR misexpression in other contexts have so far been unsuccessful (L.N, L.v.G and P.G., unpub.).

Establishing the appropriate morphology to support sensory receptor function is a general challenge for sensory cells. While the function of sensory receptors like rhodopsin are known to be necessary for sensory neuron morphogenesis (Kumar and Ready, 1995; Xiong and Bellen, 2013; Zanini et al., 2018), the current analysis demonstrates the ability of sensory receptors to play an instructive role in establishing the structural characteristics of a sensory ending. The use of a sensory receptor to specify morphology provides a simple mechanism by which the structure and function of a sensory neuron can be coordinated.

STAR Methods

CONTACT FOR REAGENT AND RESOURCE SHARING

Further information and request for resources and reagents should be directed and will be fulfilled by the Lead Contact, Paul Garrity (pgarrity@brandeis.edu)

EXPERIMENTAL MODEL AND SUBJECT DETAILS

Drosophila melanogaster flies were raised on standard cornmeal food supplemented with yeast in temperature, humidity and light controlled incubator (25^{o}C degrees, 60% relative humidity, 12hs light/12hs dark). For behavior and physiology, young (2–10 days old) female flies were used 24hs after selection using CO_2.

***Drosophila* strains:** *brv1^{L563stop}* (Gallio et al., 2011), *brv2^{W205stop}* (Gallio et al., 2011), *Ir25a-Gal4* (Benton et al., 2009)(BDSC_41728), *UAS-GCaMP6m* (P[20XUAS-IVS-GCaMP6m]attp2 and P[20XUAS-IVS-GCaMP6m]attP40 (Chen et al., 2013) (BDSC_42748), *Ir21a$^{\Delta 1}$* (Ni et al., 2016), *Ir21a^{123}* (Ni et al., 2016), *Ir25a^{2}* (Benton et al., 2009) (BDSC_41737), *Gr28b^{MB03888}* (BDSC_24190) (Ni et al., 2013), *Ir93a^{MI05555}* (Knecht et al., 2016)(BDSC_42090), *Ir21a* genomic rescue *[Ir21a^{+}]* (Ni et al., 2016), *Ir25a BAC rescue [Ir25a^{+}]* (Chen et al., 2015), *UAS-Ir93a* (Knecht et al., 2016), *Ir68a-Gal4* (Knecht et al., 2017), *UAS-Ir21a* (Ni et al., 2016), *Ir40a-Gal4* (Silbering et al., 2011) (BDSC_41727), and *GMR11F02-Gal4* (Klein et al., 2015) (BDSC_49828) were previously described. Genotypes in figure 3: *Ir21a$^{-/-}$* : *Ir21a^{123}/Ir21a^{123}*. *Ir21a* rescue: *Ir21a^{123}/Ir21a^{123}*; *[Ir21a^{+}]*. *Ir25a $^{-/-}$* : *Ir25a^{2}/Ir25a^{2}*. *Ir25a* rescue: *Ir25a^{2}/Ir25a^{2}*; *[Ir25a^{+}]*. *Ir93a$^{-/-}$* : *Ir93a^{MI05555}/Ir93a^{MI05555}*. *Ir93a$^{-/-}$* rescue : *UAS-Ir93a ;Ir93a^{MI05555}/Ir93a^{MI05555}* (UAS-IR93a drives Gal4-independent IR93a expression in the antenna(Knecht et al., 2016)). *Gr28b$^{-/-}$*: *Gr28b^{MB03888} /Gr28b^{MB03888}*. *Ir21a$^{-/-}$Gr28b$^{-/-}$*: *Ir21a^{123},Gr28b^{MB03888}/ Ir21a^{123},Gr28b^{MB03888}*.

METHOD DETAILS

Electrophysiology: 2–10 day old females, immobilized in a truncated pipette tip with head partially protruding, had arista cut with scissors (FST 15000–03) at third branch from the base. A reference tungsten electrode was inserted into the eye, and a glass recording electrode (tip larger than arista's diameter, containing 130mM NaCl, 5mM KCl, 2mM $MgCl_2$, 2mM $CaCl_2$, 36mM D-sucrose, 5mM Hepes, pH 7.3) was placed onto cut arista tip. Signals were amplified by TasteProbe DTP-02 (Syntech) and digitized using PowerLab 8/30 (ADInstruments). Temperatures were measured by using an IT-23 thermocouple (time constant 5 msec, ADInstruments) attached to a Fluke 80TK thermocouple module. The module was mounted immediately adjacent to the animal, within the same air stream as the arista. Temperature and electrophysiological data were acquired in parallel through separate channels of the PowerLab DAQ. Data were acquired with LabChart (ADInstruments) at 20k/s and band-pass filtered (100Hz-3000Hz). Two dry airstreams of differing temperature were alternated using a micromanipulator. Recordings lasted 180 seconds: for long-pulse protocol temperature was switched at 20s and 100s, for short-pulse protocol switched at 30s, 65s, 100s and 135s. Airstream was conditioned to 20˚C or 25˚C by passing the tubing through a water bath, and then divided into two branches, one warmed by a resistor (Emron E5CSV). Spikes were distinguished from background using the Peak after threshold function in Lab Chart 7, setting a voltage threshold of 3.5 times the standard deviation of voltage signals determined in spike-free regions of the recording. Spike rates were calculated as the weighted average of Instantaneous Spike Frequencies across a Triangular Bartlett window centered at the time indicated; a 1 sec window was used in all analyses, except in Supp. Fig. 1B, where a 100 msec window was used for enhanced temporal resolution. Cooling response was calculated as the difference between the average spike frequency of the first 2 sec of cooling and the average spike frequency over the 10 sec prior to cooling.

Specimen preparation for electron microscopy: The third antennal segment (funiculus), arista attached, was removed from CO_2-anesthetized flies using fine tweezers. The arista tip was cut off (distal to thermoreceptor endings) with iridectomy scissors to enhance fixative penetration. Immediately after dissection, 2–4 funiculi were embedded in a pad of 2.4% low-melting point agarose (at RT) inside the cavity of a type 'A' aluminum high-pressure freezer planchette with 100 μm depth (Wohlwend, Switzerland). The flat surface of a type 'B' planchette was placed on top to enclose the samples. The planchette sandwich was rapidly frozen using a Leica EM HPM100 high-pressure freezing system (Leica Microsystems, Vienna, Austria). Freeze-substitution was performed at low temperature (−90°C) over 3–4 days in 1% osmium tetroxide (19,100 from EMS), 0.5% glutaraldehyde (16,530 from EMS) and 2% water in anhydrous acetone (AC32680–1000, Fisher) using a Leica EM AFS2 freeze-substitution system. The temperature was increased to 0°C (5°C/hr), and finally brought to 4°C and maintained at this temperature for 1 hr. Samples were washed four times with anhydrous acetone (30 min each), then infiltrated and flat embedded in Araldite 502/Embed-812 resin (Araldite: 10,900; Embed-812: 14,900; DDSA: 13,710; all from EMS) at room temperature and polymerized in an oven at 60°C for 3–4 days. After initial flat embedding, the arista samples were later re-embedded in an orientation optimized for cross-sectioning the arista.

Serial section Transmission Electron Microscopy: For each arista, several hundred serial ultrathin sections (70 nm thickness) were collected on Formvar-coated slot grids, post-stained with a saturated solution of uranyl acetate (0379, Polysciences, Inc., Warrington, PA) for 15 min and Reynold's lead citrate (Lead nitrate: 17,900 from EMS; Sodium citrate: S-279 from Fisher) for 7 min. Serial sections were studied using a Tecnai F20 (200 keV) transmission electron microscope (FEI, Hillsboro, OR) and images were recorded using a 2K × 2K charged-coupled device camera (Gatan) at 19,000x magnification (1.12 nm pixel size). Each arista was imaged at multiple levels to obtain a full picture of the changes that occur along the length of the sensilla. In each experiment, one arista was reconstructed per animal. For wild type: one animal was serial sectioned and imaged to confirm that thermoreceptor morphology was as previously reported (Foelix et al., 1989). As there are three sensilla per arista, 3 Cooling Cells and 3 Hot Cells were examined. Their morphology was as previously reported (Foelix et al., 1989), so additional wild type were not reconstructed. For *Ir21a* and *Ir25a* mutants, 3 animals of each genotype were serial sectioned and imaged, so that a total of 9 Cooling Cells and 9 Hot Cells were examined per genotype. The reported phenotypes were fully penetrant. For ectopic IR21a expression, 3 animals (totaling 9 Hot Cells and 9 Cooling Cells) were serial sectioned and imaged. In each animal, IR21a was expressed in both Hot Cells and Cooling Cells under GMR11F02-Gal4 control. In two animals, this expression was performed in an *Ir21a* null mutant background (providing both rescue and ectopic expression), while in the third animal IR21a was expressed in an otherwise *wild type* background. The reported phenotypes were fully penetrant and similar across the animals examined.

Immunohistochemistry: Aristae, distal portions removed prior to fixation, were stained as described (Knecht et al., 2017). Primary antibodies were: guinea pig anti-IR21a, peptide epitope: EDEESREALESLQRLDEFMD (1:100, Proteintech, Chicago), rabbit anti-IR25a (1:100) (Benton et al., 2009), rabbit anti-IR93a (1:100)(Knecht et al., 2016), chicken anti-GFP (1:1000, Abcam 13970), and mouse anti-E7 tubulin beta (1:100, DSHB). Secondary antibodies (used at 1:200) were: goat anti-chicken Alexa 488 (A-11039, Life Technologies), goat anti-mouse Alexa 488 (A11029, Invitrogen), goat anti-guinea pig Cy3 (Jackson ImmunoResearch), and goat anti-rabbit Cy3 (Jackson ImmunoResearch). Images were obtained on Leica Sp5 confocal or Nikon A1 confocal and processed using FIJI and Adobe Photoshop. For the fluorescence immunostaining in Figure 4A: n=8 samples for *wild type*; n=10 for *Ir21a* mutants, n= 9 for *Ir25a* mutants and n=4 for *Ir93a* mutants.

DNA sequencing: For DNA sequencing: *brv1* primers were 5'-GCGTTTGTGGAAAGTGTTGCAG and 5'GTGGGCATATTCAACGCGCAG, and *brv2* primers were 5'-CACAGCTATATGAAGATCACC and 5'-GGTATTCGATCTGCTTCAAGC.

Calcium imaging: Calcium imaging was performed as described (Klein et al., 2015). Data was collected at 4 frames per second. F_0 was the initial data point. Cooling responses in Supplemental Figure 4D were calculated as [F/F_0 at 21˚C (average F/F_0 from 2.5 to 7.5 s after shift to 21˚C)] - [F/F_0 at 25˚C (average F/F_0 from 5.25 to 3 s prior to shift to 21˚C)].

Warming responses in Supplemental Figure 4D were calculated using the converse calculation.

QUANTIFICATION AND STATISTICAL ANALYSIS

Normality of distributions was assessed by Shapiro-Wilk W test ($p \leq 0.05$ rejected normal distribution). Statistical comparisons of normally distributed data were performed by unpaired t-test or, for multiple comparisons, Tukey HSD. For data that did not conform to a normal distribution, statistical comparisons were performed by Wilcoxon or, for multiple comparisons, Steel with control and Steel-Dwass tests. All tests performed using JMP11 (SAS).

Supplementary Material

Refer to Web version on PubMed Central for supplementary material.

Acknowledgements:

We acknowledge the Bloomington *Drosophila* Stock Center (NIH P40OD018537) and the Developmental Studies Hybridoma Bank (NICHD of the NIH, University of Iowa) for reagents. We thank Willem Laursen, Amy Lee and Michael Rosbash for comments on the manuscript. This work was supported by grants from the National Institute of General Medicine (F32 GM113318) and National Institute of Neurological Disorders and Strokes (T32-NS007292) to G.B., the National Institute on Deafness and Other Communication Disorders (F31 DC015155) to Z.A.K., the Swiss National Science Foundation (P2FRP3_168480) to L. v. G, European Research Council Starting Independent Researcher and Consolidator Grants (205202 and 615094) to R.B., the National Institute of General Medical Sciences (R01 GM083122) to D.N. the National Institute of General Medical Sciences (P01 GM103770) to A.D.T and P.A.G, the National Science Foundation (IOS 1557781) to P.A.G. and the National Institute of Allergy and Infectious Diseases (R01 AI122802) to P.A.G. This work was also supported by a grant from the National Science Foundation (IOS 1557781) to P.A.G.

References:

Altner H, and Loftus R (1985). Ultrastructure and function of insect thermo- and hygroreceptors. Ann Rev Entomol 30, 273–295.

Bagriantsev SN, and Gracheva EO (2014). Molecular mechanisms of temperature adaptation. The Journal of physiology doi: 10.1113/jphysiol.2014.280446

Barbagallo B, and Garrity PA (2015). Temperature sensation in Drosophila. Current opinion in neurobiology 34C, 8–13. doi: 10.1016/j.conb.2015.01.002

Benton R, Vannice KS, Gomez-Diaz C, and Vosshall LB (2009). Variant ionotropic glutamate receptors as chemosensory receptors in Drosophila. Cell 136, 149–162. [PubMed: 19135896]

Biron D, Wasserman S, Thomas JH, Samuel AD, and Sengupta P (2008). An olfactory neuron responds stochastically to temperature and modulates Caenorhabditis elegans thermotactic behavior. Proceedings of the National Academy of Sciences of the United States of America 105, 11002–11007. doi: 10.1073/pnas.0805004105 [PubMed: 18667708]

Chen C, Buhl E, Xu M, Croset V, Rees JS, Lilley KS, Benton R, Hodge JJ, and Stanewsky R (2015). Drosophila Ionotropic Receptor 25a mediates circadian clock resetting by temperature. Nature 527, 516–520. doi: 10.1038/nature16148 [PubMed: 26580016]

Chen TW, Wardill TJ, Sun Y, Pulver SR, Renninger SL, Baohan A, Schreiter ER, Kerr RA, Orger MB, Jayaraman V, et al. (2013). Ultrasensitive fluorescent proteins for imaging neuronal activity. Nature 499, 295–300. doi: 10.1038/nature12354 [PubMed: 23868258]

Croset V, Rytz R, Cummins SF, Budd A, Brawand D, Kaessmann H, Gibson TJ, and Benton R (2010). Ancient protostome origin of chemosensory ionotropic glutamate receptors and the evolution of insect taste and olfaction. PLoS genetics 6, e1001064. doi: 10.1371/journal.pgen.1001064 [PubMed: 20808886]

Dell AI, Pawar S, and Savage VM (2011). Systematic variation in the temperature dependence of physiological and ecological traits. Proceedings of the National Academy of Sciences of the United States of America 108, 10591–10596. doi: 10.1073/pnas.1015178108 [PubMed: 21606358]

Dong X, Shen K, and Bulow HE (2015). Intrinsic and extrinsic mechanisms of dendritic morphogenesis. Annual review of physiology 77, 271–300. doi: 10.1146/annurev-physiol-021014-071746

Ehn R, and Tichy H (1996). Response characteristics of a spider warm cell: temperature sensitivities and structural properties. J Comp Physiol A 178, 537–542.:

Enjin A, Zaharieva EE, Frank DD, Mansourian S, Suh GS, Gallio M, and Stensmyr MC (2016). Humidity sensing in Drosophila. Current biology : CB 26, 1352–1358. doi: 10.1016/j.cub.2016.03.049 [PubMed: 27161501]

Foelix RF, Stocker RF, and Steinbrecht RA (1989). Fine structure of a sensory organ in the arista of Drosophila melanogaster and some other dipterans. Cell and tissue research 258, 277–287. [PubMed: 2510932]

Frank DD, Enjin A, Jouandet GC, Zaharieva EE, Para A, Stensmyr MC, and Gallio M (2017). Early intergration of temperature and humidity stimuli in the Drosophila brain. Current Biology 27, 1–8. doi: 10.1016/j.cub.2017.06.077 [PubMed: 27916526]

Frank DD, Jouandet GC, Kearney PJ, Macpherson LJ, and Gallio M (2015). Temperature representation in the Drosophila brain. Nature 519, 358–361. doi: 10.1038/nature14284 [PubMed: 25739506]

Gallio M, Ofstad TA, Macpherson LJ, Wang JW, and Zuker CS (2011). The coding of temperature in the Drosophila brain. Cell 144, 614–624. doi: 10.1016/j.cell.2011.01.028 [PubMed: 21335241]

Goris RC (2011). Infrared organs of snakes: an integral part of vision. J Herpetology 45, 2–14.

Haesemeyer M, Robson DN, Li JM, Schier AF, and Engert F (2018). A Brain-wide Circuit Model of Heat-Evoked Swimming Behavior in Larval Zebrafish. Neuron 98, 817–831 10.1016/j.neuron.2018.04.013 [PubMed: 29731253]

Hamada FN, Rosenzweig M, Kang K, Pulver SR, Ghezzi A, Jegla TJ, and Garrity PA (2008). An internal thermal sensor controlling temperature preference in Drosophila. Nature 454, 217–220. 10.1038/nature07001 [PubMed: 18548007]

Hensel H (1976). Functional and structural basis of thermoreception. Progress in brain research 43, 105–118. doi: 10.1016/S0079-6123(08)64343-5 [PubMed: 815955]

Jan YN, and Jan LY (2010). Branching out: mechanisms of dendritic arborization. Nature Reviews Neuroscience 11, 316–328. doi: doi:10.1038/nrn2836 [PubMed: 20404840]

Kamm GB, and Siemens J (2017). The TRPM2 channel in temperature detection and thermoregulation. Temperature 4, 21–23. doi: 10.1080/23328940.2016.1258445

Klein M, Afonso B, Vonner AJ, Hernandez-Nunez L, Berck M, Tabone CJ, Kane EA, Pieribone VA, Nitabach MN, Cardona A, et al. (2015). Sensory determinants of behavioral dynamics in Drosophila thermotaxis. Proceedings of the National Academy of Sciences of the United States of America 112, E220–229. doi: 10.1073/pnas.1416212112 [PubMed: 25550513]

Knecht ZA, Silbering A, Cruz J, Yang L, Croset V, Benton R, and Garrity PA (2017). Ionotropic Receptor-dependent moist and dry cells control hygrosensation in Drosophila. eLife 6. doi: 10.7554/eLife.26654

Knecht ZA, Silbering AF, Ni L, Klein M, Budelli G, Bell R, Abuin L, Ferrer AJ, Samuel AD, Benton R, et al. (2016). Distinct combinations of variant ionotropic glutamate receptors mediate thermosensation and hygrosensation in Drosophila. eLife 5. doi: 10.7554/eLife.17879

Kuhara A, Okumura M, Kimata T, Tanizawa Y, Takano R, Kimura KD, Inada H, Matsumoto K, and Mori I (2008). Temperature sensing by an olfactory neuron in a circuit controlling behavior of C. elegans. Science 320, 803–807. doi: 10.1126/science.1148922 [PubMed: 18403676]

Kumar JP, and Ready DF (1995). Rhodopsin plays an essential structural role in Drosophila photoreceptor development. Development 121, 4359–4370. doi: [PubMed: 8575336]

Liu WW, Mazor O, and Wilson RI (2015). Thermosensory processing in the Drosophila brain. Nature 519, 353–357. doi: 10.1038/nature14170 [PubMed: 25739502]

Mori I, and Ohshima Y (1995). Neural regulation of thermotaxis in Caenorhabditis elegans. Nature 376, 344–348. [PubMed: 7630402]

Morrison SF (2016). Central control of body temperature. F1000Research 5. doi: 10.12688/f1000research.7958.1

Munger BL, and Ide C (1988). The structure and function of cutaneous sensory receptors. Archives of histology and cytology 51, 1–34. [PubMed: 3137944]

Ni L, Bronk P, Chang EC, Lowell AM, Flam JO, Panzano VC, Theobald DL, Griffith LC, and Garrity PA (2013). A gustatory receptor paralogue controls rapid warmth avoidance in Drosophila. Nature 500, 580–584. doi: 10.1038/nature12390 [PubMed: 23925112]

Ni L, Klein M, Svec KV, Budelli G, Chang EC, Ferrer AJ, Benton R, Samuel AD, and Garrity PA (2016). The Ionotropic Receptors IR21a and IR25a mediate cool sensing in Drosophila. eLife 5. doi: 10.7554/eLife.13254

Palkar R, Lippoldt EK, and McKemy DD (2015). The molecular and cellular basis of thermosensation in mammals. Current opinion in neurobiology 34, 14–19. doi: 10.1016/j.conb.2015.01.010 [PubMed: 25622298]

Ramot D, MacInnis BL, and Goodman MB (2008). Bidirectional temperature-sensing by a single thermosensory neuron in C. elegans. Nature neuroscience 11, 908–915. [PubMed: 18660808]

Ruchty M, Roces F, and Kleineidam CJ (2010). Detection of minute temperature transients by thermosensitive neurons in ants. Journal of neurophysiology 104, 1249–1256. doi: 10.1152/jn.00390.2010 [PubMed: 20573968]

Rytz R, Croset V, and Benton R (2013). Ionotropic receptors (IRs): chemosensory ionotropic glutamate receptors in Drosophila and beyond. Insect biochemistry and molecular biology 43, 888–897. doi: 10.1016/j.ibmb.2013.02.007 [PubMed: 23459169]

Silbering AF, Rytz R, Grosjean Y, Abuin L, Ramdya P, Jefferis GS, and Benton R (2011). Complementary function and integrated wiring of the evolutionarily distinct Drosophila olfactory subsystems. J Neurosci 31, 13357–13375. doi: 10.1523/JNEUROSCI.2360-11.2011 [PubMed: 21940430]

Steinbrecht RA (1989). The fine structure of thermo-/hygrosensitive sensilla in the silkmoth Bombyx mori: Receptor membrane substructure and sensory cell contacts. Cell and tissue research 255, 49–57.

van Giesen L, and Garrity PA (2017). More than meets the IR: the expanding roles of variant Ionotropic Glutamate Receptors in sensing odor, taste, temperature and moisture. F1000Research 6, 1753. doi: 10.12688/f1000research.12013.1 [PubMed: 29034089]

Vriens J, Nilius B, and Voets T (2014). Peripheral thermosensation in mammals. Nature reviews Neuroscience 15, 573–589. doi: 10.1038/nrn3784 [PubMed: 25053448]

Wu H, Williams J, and Nathans J (2012). Morphologic diversity of cutaneous sensory afferents revealed by genetically directed sparse labeling. eLife 1, e00181. doi: 10.7554/eLife.00181 [PubMed: 23256042]

Xiong B, and Bellen HJ (2013). Rhodopsin homeostasis and retinal degeneration: lessons from the fly. Trends in neurosciences 36, 652–660. doi: 10.1016/j.tins.2013.08.003 [PubMed: 24012059]

Zanini D, Giraldo D, Warren B, Katana R, Andres M, Reddy S, Pauls S, Schwedhelm-Domeyer N, Geurten BRH, and Gopfert MC (2018). Proprioceptive Opsin Functions in Drosophila Larval Locomotion. Neuron 98, 67–74 10.1016/j.neuron.2018.02.028 [PubMed: 29551493]

Highlights:

1. Key drivers of *Drosophila* thermosensing detect heating and cooling, not hot and cold.
2. Ionotropic Receptors (IRs), not Brivido TRP channels, mediate cooling detection.
3. IRs specify both the morphogenesis and thermosensitivity of sensory endings.
4. Thermoregulation requires context-dependent interpretation of phasic sensory inputs.

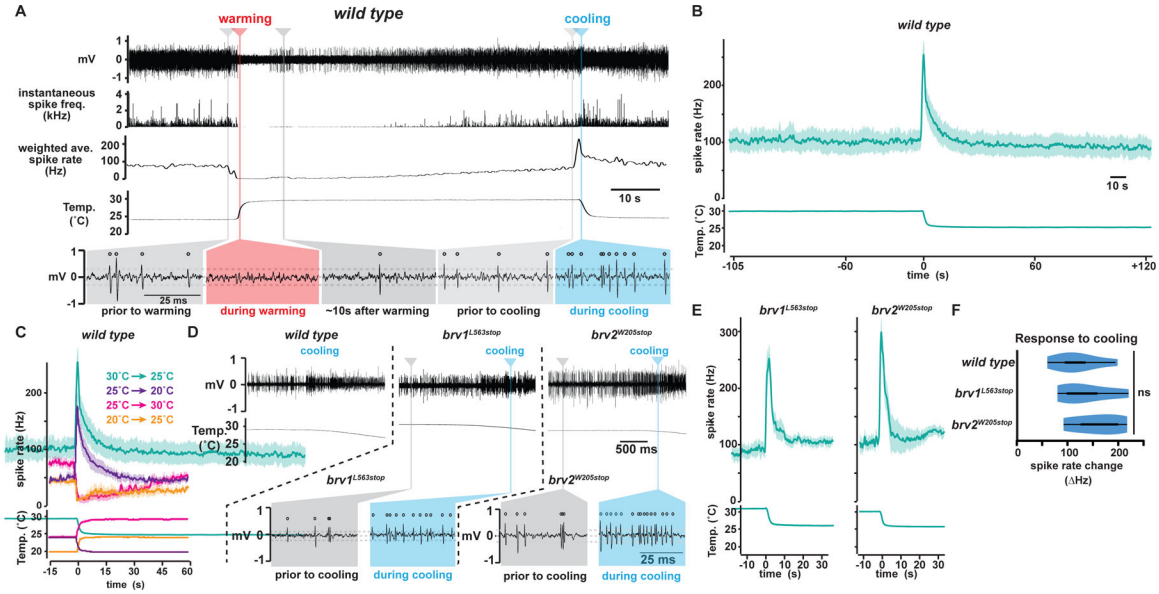

Fig. 1. Cold Cells are Brivido-independent phasic thermoreceptors.

A,Representative recording from a *wild type* arista. In upper panels, instantaneous spike frequency was smoothed using a 1s triangular window to generate weighted average spike rate. Lower panels show data from upper panels displayed on expanded time scale, revealing individual spikes (open circles). Spike voltage threshold of 3.5 times the standard deviation of spike-free regions of recording indicated by dotted lines. **B, C,** Peristimulus time histograms (PSTHs) of responses from *wild type* aristae (n=7 animals per condition; one trial per animal). Average +/− SEM. In panel C, results of four different temperature steps are superimposed. **D**, Upper panels show representative recordings from *wild type*, $brv1^{L563stop}$, and $brv2^{W205stop}$ aristae. In lower panels, data from upper panels is displayed on expanded time scale, as in **A**. **E**, PSTHs from $brv1^{L563stop}$ n=6) and $brv2^{W205stop}$ (n=7) recordings. **F,** Cooling response quantification: cooling response = (average spike rate during first 2 sec of 30˚C to 25˚C cooling) – (average spike rate, 10 sec pre-cooling). *wild type*, n=8 animals, $brv1^{L563stop}$, n=6, $brv2^{W205stop}$, n=7. In violin plots, white circles represent median, black boxes denote 25th to 75th percentiles, and whiskers extend 1.5x interquartile range. See also Supplemental Figures 1 and 2.

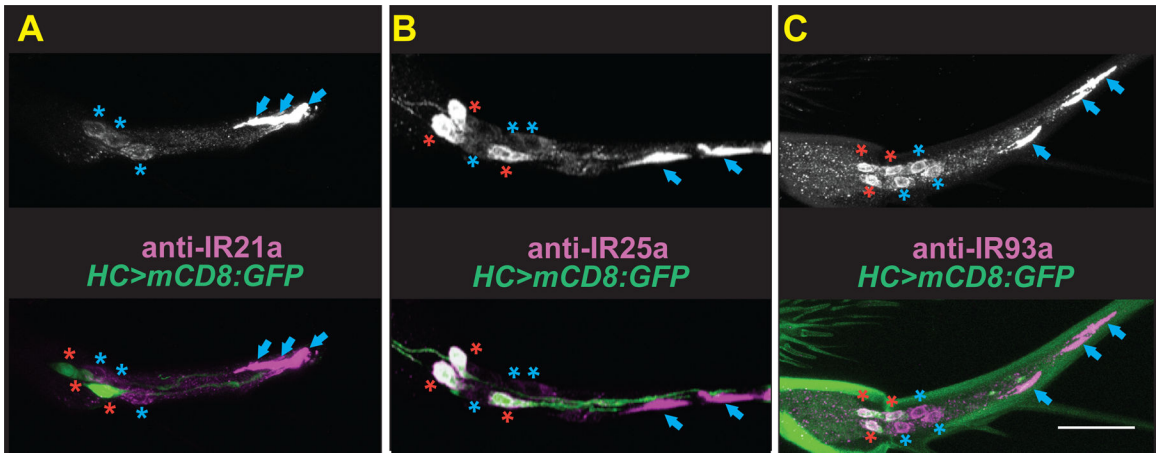

Fig. 2. IR21a, IR25a and IR93a proteins localize to Cold Cell sensory endings.

A-C, IR21a (**A**), IR25a (**B**), and IR93a (**C**) immunostaining. Top panels, anti-IR immunostaining. Bottom, merge with Hot Cell-specific *HC-Gal4;UAS-GFP*. Blue asterisks, Cold Cells. Red asterisks, Hot Cells. Blue arrows, Cold Cell outer segments. See also Supplemental Figure 3.

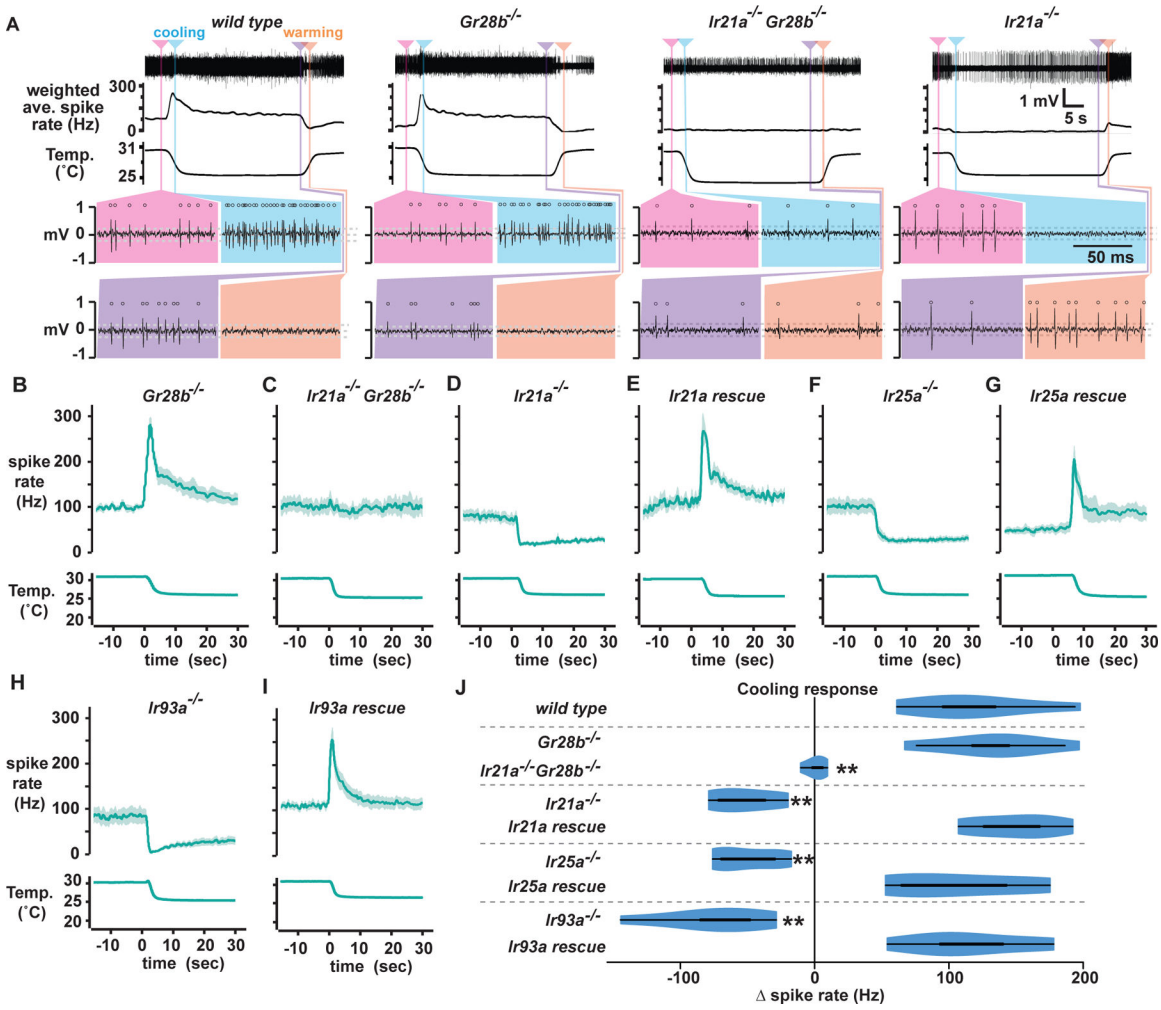

Fig. 3. *Ir21a*, *Ir25a* and *Ir93a* are required for Cold Cell thermosensing.

A, Representative recordings from indicated genotypes, with indicated portions displayed below using an expanded time scale, as in Fig. 1. **B-I**,PSTHs of temperature responses. (**J)** Cooling response quantification as in Fig. 1. Genotypes detailed in methods. **alpha=0.01, distinct from *wild type*, Tukey HSD (n=6 or 7 animals per genotype). See also Supplemental Figures 4 and 5.

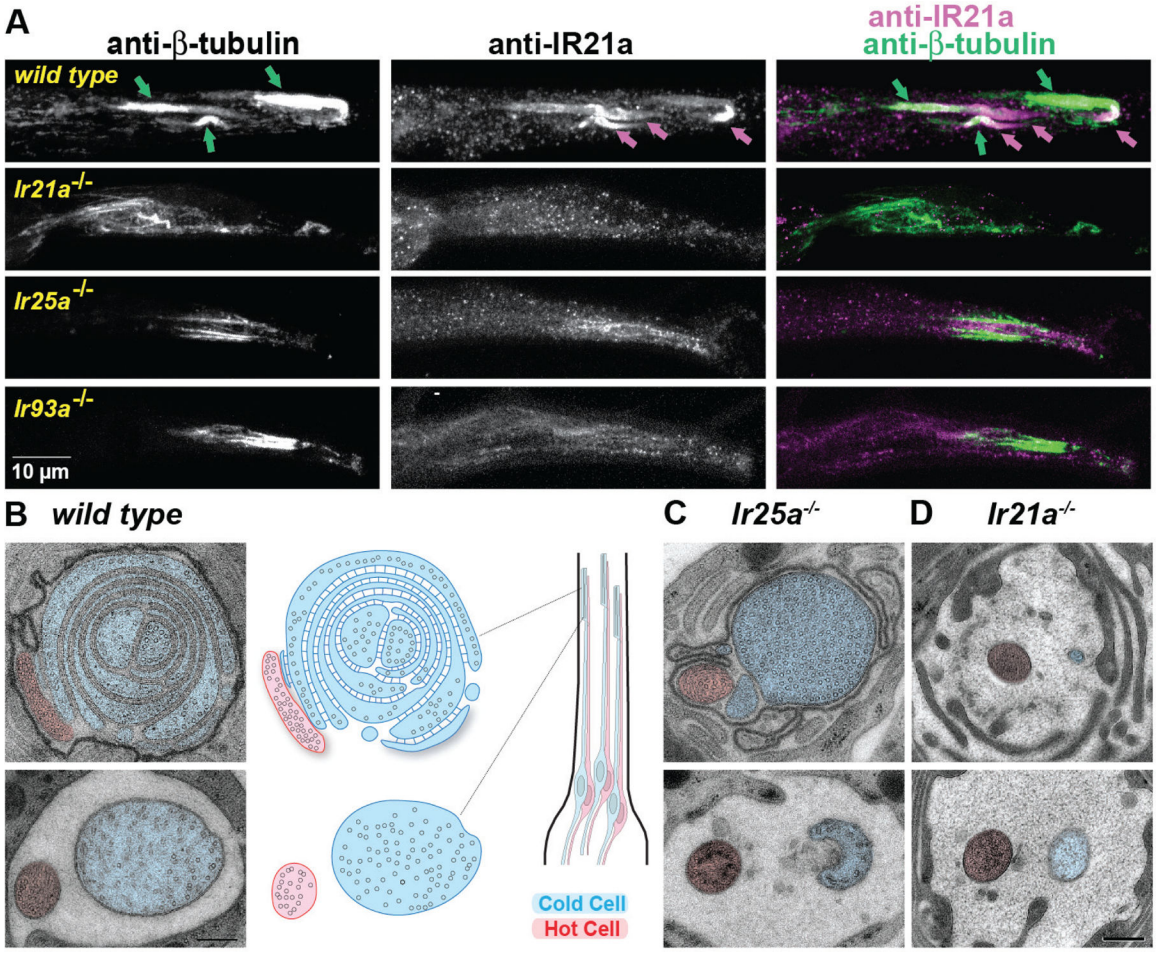

Fig. 4. IRs are required for thermoreceptor morphogenesis.

A. Arista immunostaining. Merge: Green, beta-tubulin; magenta, IR21a. Green arrows denote tubulin staining and magenta arrows denote IR21a staining of thermoreceptor sensory endings. **B-D,** EM sections through arista sensilla. Hot Cell, red shading. Cold Cell, blue shading. Upper panels, sections nearer sensillum's distal tip. Strains: $Ir21a^{-/-}$: $Ir21a^{\Delta 1}/Ir21a^{\Delta 1}$. $Ir25a^{-/-}$: $Ir25a^{2}/Ir25a^{2}$. $Ir93a^{-/-}$: $Ir93a^{MI05555}/Ir93a^{MI05555}$. **B,** Left panel, transmission electron micrographs. Middle, drawing depicts microtubules (circles) and "BOSS" structures (thin lines) between Cold Cell membranes. Right, drawing depicts arista thermoreceptor pairs and approximate micrograph locations. **C,D,** Representative electron micrographs of similar locations (upper panels, more distal) in $Ir25a^{-/-}$ and $Ir21a^{-/-}$. Scale bar: panel A, 10 µm, panels B-D, 200 nm.

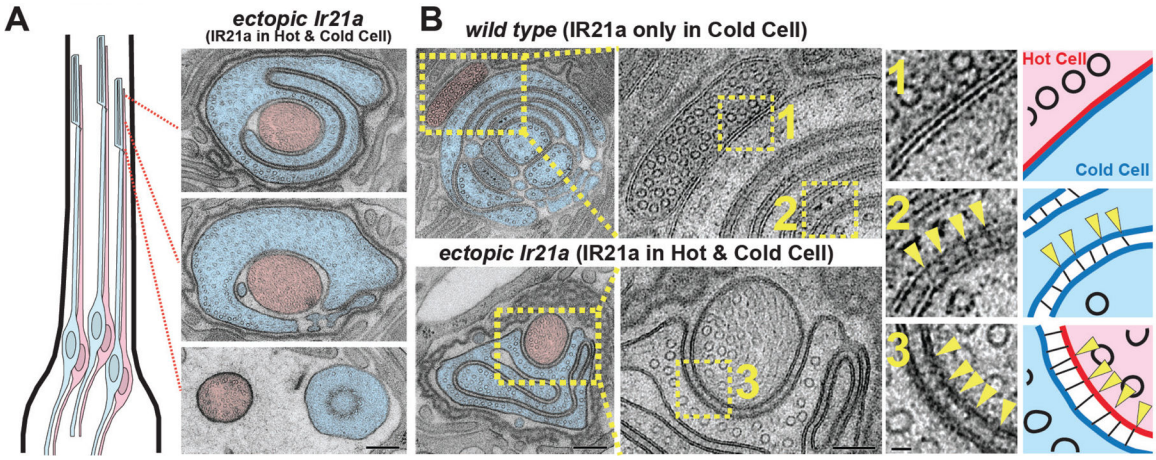

Fig. 5. Ectopic IR21a expression alters thermoreceptor morphology.

A, Left panel, drawing of arista indicating approximate locations of adjacent electron micrographs. Right panels, representative transmission electron micrograph of animals expressing IR21a in both Hot and Cold Cells: *Ir21a*$^{\Delta 1}$/*Ir21a*$^{\Delta 1}$;*GMR11F02-Gal4/UAS-Ir21a*. Cold Cell, blue. Hot Cell, red. **B**, EM sections through wild-type and *GMR11F02>Ir21a* animals, near distal tip of sensory endings. Middle panels represent inset region of left panels. Right panels represent the numbered insets from middle panels. Yellow arrowheads denote high magnification views of BOSS structures between membranes. Scale bars: A (right panels) and B (left panels), 200 nm; B (middle panels), 100 nm; B (right panels), 20 nm. See also Supplemental Figure 6.

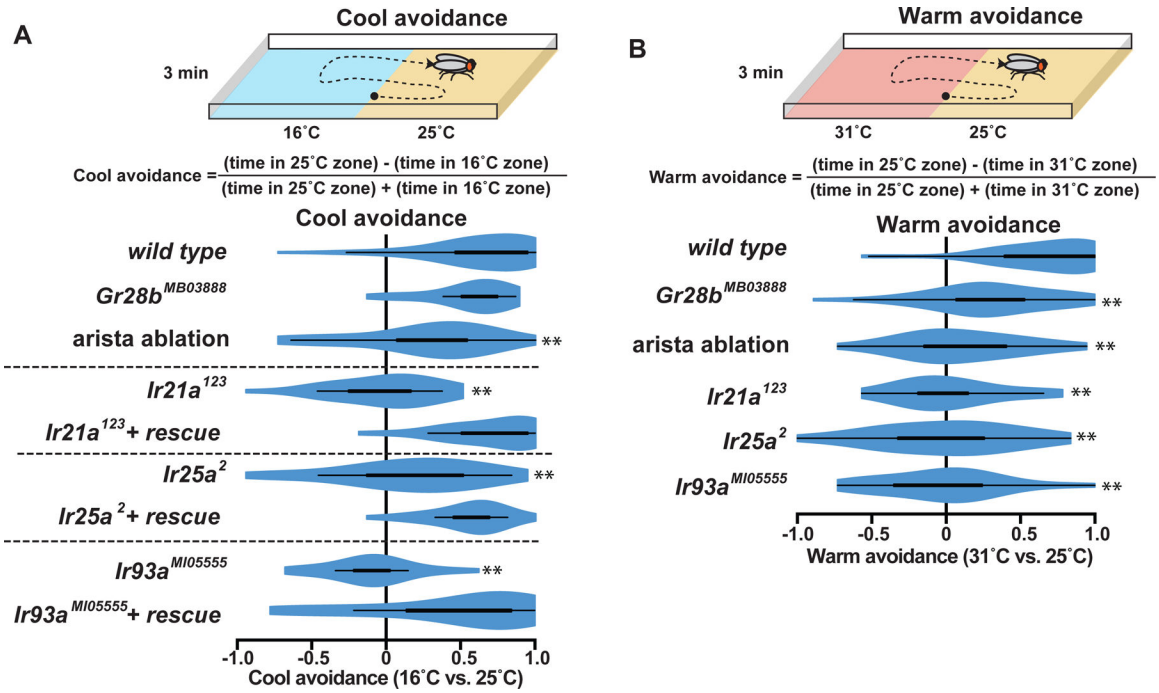

Figure 6: Ionotropic Receptors mediate both cool and warm avoidance.

A, Top panel, cool avoidance assay schematic. Bottom panel, cool avoidance of indicated genotypes. **B**, Top panel, warm avoidance assay schematic. Bottom panel, warm avoidance of indicated genotypes. ** P<0.01 distinct from *wild type*, Steel with control. n=24 individuals assayed for each genotype and condition, except n=48 for *wild type,* arista ablation cool avoidance and *Gr28b*^{MB03888} warm avoidance.

KEY RESOURCES TABLE

REAGENT or RESOURCE	SOURCE	IDENTIFIER
Fly strains		
$brv1^{L563stop}$	Gallio *et al.* (2011)	
$brv2^{W205stop}$	Gallio *et al.* (2011)	
Ir25a-Gal4	Benton *et al.*, 2009	BDSC_41728
UAS-GCaMP6m (P[20XUAS-IVS-GCaMP6m]attp2)	Chen *et al.*, 2013	
UAS-GCaMP6m (P[20XUAS-IVS-GCaMP6m]attp40)	Chen *et al.*, 2013	BDSC_42748
$Ir21a^{\Delta 1}$	Ni *et al.*, 2016	
$Ir21a^{123}$	Ni *et al.*, 2016	
$Ir25a^{2}$	Benton *et al.*, 2009	BDSC_41737
$Gr28b^{MB03888}$	Ni *et al.*, 2013	BDSC_24190
$Ir93a^{MI05555}$	Knecht et al., 2016	BDSC_42090
Ir21a genomic rescue [$Ir21a^{+}$]	Ni *et al., 2016*	
Ir25a BAC rescue [$Ir25a^{+}$]	Chen *et al., 2015*	
UAS-Ir93a	Knecht *et al., 2016*	
Ir68a-Gal4	Knecht *et al.*, 2017	
UAS-Ir21a	Ni *et al.*, 2016	
Ir40a-Gal4	Silbering *et al.*, 2011	BDSC_41727
GMR11F02-Gal4	Klein *et al.*, 2015	BDSC_49828
Antibodies		
anti-IR21a (guinea pig)	Proteintech, Chicago	
anti-IR25a (rabbit)	Benton *et al.*, 2009	
anti-IR93a (rabbit)	Knecht *et al.*, 2016	
anti-GFP (chicken)	Abcam	13970
anti-tubulin beta E7 (mouse)	DSHB	AB_2315513
anti-chicken Alexa 488 (goat)	Life Technologies	A-11039
anti-mouse Alexa 488 (goat)	Invitrogen	A-11029
anti-guinea pig Cy3 (goat)	Jackson ImmunoResearch	1067165003
Anti-rabbit Cy3 (goat)	Jackson ImmunoResearch	111165003
Software		
LabChart	ADInstruments	Pro V7
FIJI	ImageJ	Version 2.0.0
Photoshop	Adobe	
Excel	Microsoft	
JMP	SAS	
Arista imaging code	https://github.com/masonklein/neurophys/	